



Iranian Research Organization
for Science and Technology
(IROST)

Advances
Environmental
Technology



Journal home page: <https://aet.irost.ir>

Easy one-pot synthesis of Zinc Ferrite@Graphitic Carbon Nitride for combined adsorption and photocatalytic degradation of enrofloxacin under visible light

Muchammad Tamyiz^{*a}, Medya Ayunda Fitri^b, Zahrotul Azizah^b, Nabila Nur Fauziyah Putri Asmarani^a, Inayah Nuzulil Rahma^a

^aDepartment of Environmental Engineering, Faculty of Engineering, Universitas Nahdlatul Ulama Sidoarjo, Indonesia

^bDepartment of Chemical Engineering, Faculty of Engineering, Universitas Nahdlatul Ulama Sidoarjo, Indonesia

ARTICLE INFO

Document Type:
Research Paper

Article history:
Received 01 October 2024
Received in revised form
28 March 2025
Accepted 30 March 2025

Keywords:
Enrofloxacin degradation
Graphitic carbon nitride (g-C₃N₄)
Nanocomposite
Photocatalysis
Zinc ferrite (ZnFe₂O₄).

ABSTRACT

This study explores the development and application of an eco-friendly nanocomposite, OP-ZF@CN, for the degradation of enrofloxacin (ENR) in water. Antibiotics like ENR are persistent environmental pollutants, and conventional wastewater treatments are insufficient for their removal. Photocatalysis has emerged as a promising solution, offering a cost-effective, non-toxic, and efficient method for degrading contaminants. In this work, a heterojunction was formed between graphitic carbon nitride (g-C₃N₄, 2DCN) and zinc ferrite (ZnFe₂O₄, ZF), synthesized through a one-pot hydrothermal method. The resulting OP-ZF@CN nanocomposite combines the advantages of both components, improving photocatalytic performance by reducing the bandgap of 2DCN from 2.83 eV to 2.60 eV. Characterization using X-ray diffraction (XRD), scanning electron microscopy (SEM), and Fourier-transform infrared spectroscopy (FT-IR) confirmed the successful formation of the heterojunction, with ZF nanoparticles evenly distributed on the CN surface. The photocatalytic degradation of ENR was assessed under visible light, showing that OP-ZF@CN achieved a 99% degradation rate, significantly outperforming pure 2DCN and ZF. The enhanced performance could be attributed to the synergistic interaction between adsorption and photocatalysis, with rapid adsorption reaching equilibrium within 30 minutes. The adsorption capacity of OP-ZF@CN was found to be 62.23 mg g⁻¹, as determined by Langmuir and Sips isotherm models. Additionally, the nanocomposite exhibited high photocatalytic efficiency, removing ENR 10 times faster than 2DCN alone. The study also demonstrated that OP-ZF@CN had a maximum adsorption capacity of 11.08 mg g⁻¹ in a 10 mg L⁻¹ ENR solution, significantly improving adsorption compared to pure 2DCN. These results were further supported by kinetic

*Corresponding author Tel.: 085655333861

E-mail: m_tamyiz.tkl@unusida.ac.id

DOI: 10.22104/AET.2025.7146.1966

COPYRIGHTS: ©2024 Advances in Environmental Technology (AET). This article is an open access article distributed under the terms and conditions of the Creative Commons Attribution 4.0 International (CC BY 4.0) (<https://creativecommons.org/licenses/by/4.0/>)

studies, indicating that the adsorption process followed pseudo-first-order kinetics. These findings suggest that OP-ZF@CN is a highly effective material for environmental applications, particularly in wastewater treatment for antibiotic removal, with a promising potential for large-scale use.

1. Introduction

The need for pharmaceuticals, particularly antibiotics, is crucial, yet it also leads to environmental pollution [1]. Traditional wastewater treatment methods, such as filtration, coagulation, and sedimentation, struggle to degrade antibiotics like enrofloxacin (ENR) effectively [2-4]. Photocatalysis has become a promising method for pollutant degradation because of its affordability, high efficiency, environmental friendliness, and non-toxic nature while also minimizing secondary pollution [5-8]. This technique has been shown to be effective in breaking down various antibiotics, including ciprofloxacin, enrofloxacin, oxytetracycline, and sulfamethazine [1,4,9,10]. Among the potential photocatalysts, graphitic carbon nitride (g-C₃N₄, CN) has demonstrated its versatility as a material in various applications, including carbon dioxide reduction, H₂ evolution, and the removal of emerging contaminants [4,11-13]. It has unique properties such as excellent chemical stability, tunable electronic structure, visible light absorption capabilities of 2.7 eV, stability, non-toxicity, cost-effectiveness, and ease of large-scale production [14].

When CN is modified into a two-dimensional nanosheet (2DCN), it offers additional benefits, such as a greater specific surface area and reduced layer thickness [15]. The increased surface area allows for more active sites and improves the efficiency of separating photo-generated electron-hole pairs (e⁻-h⁺). However, 2DCN faces challenges, including limited visible light absorption and lower electron-hole separation rates, which hinder its photocatalytic performance [15-17]. To overcome these issues, creating heterojunctions with other photocatalysts has been found to enhance photocatalytic efficiency significantly. On the other hand, single metal oxides display lower photocatalytic efficiency under visible light compared to bimetallic oxides [18]. A specific type of bimetallic oxide, known as

spinel ferrite, is attracting attention for its nature stability, versatile magnetic properties, and distinct optical features. The ZF are particularly appealing because of their sustainable synthesis, controlled stoichiometry, small particle size, narrow bandgap of approximately 1.9 eV, and the potential for large-scale production [19,20]. Despite these benefits, pure ZF shows low photocatalytic efficiency as a result of the rapid recombination of electron-hole pairs [21]. This challenge can be mitigated by forming heterojunctions with other materials. In this research, the OP-ZF@CN nanocomposite was effectively synthesized through a hydrothermal method, showcasing a synergistic interaction between adsorption and photocatalysis for the degradation of enrofloxacin. The incorporation of ZF in the composite reduced the broad bandgap of 2DCN (2.83 eV) to 2.60 eV; this synergy enables increased light absorption and improved photodegradation of ENR. The OP-ZF@CN nanocomposite proved to be highly suitable for environmental applications.

2. Material and Methods

2.1 Material

The substances utilized in this study consist of CON₂H₄, 99% (J.T. Baker), C₂H₄N₄, 99% (Alfa Aesar), Iron(III) nitrate-9-hydrate (Riedel-de Haën), C₂H₆O, ≥ 99.8% (Sigma-Aldrich), KHSO₅•0.5KHSO₄•0.5K₂SO₄, (Sigma-Aldrich), zinc nitrate hexahydrate (J.T. Baker), C₁₉H₂₂FN₃O₃, 98% (Sigma-Aldrich), sodium azide (Alfa Aesar), p-BQ, > 99% (Sigma-Aldrich), ammonium oxalate (Sigma-Aldrich), C₃H₈O, ≥ 99% (Sigma-Aldrich), CH₃OH 99.9% (Sigma-Aldrich), CH₃CN (Sigma-Aldrich), CH₂O₂, 95% (J.T. Baker), Na₂SO₄ 99% (J.T. Baker), HCl (J.T. Baker), NaOH (J.T. Baker), and distilled water. All chemicals were utilized as received without any additional purification.

2.2 Synthesis of OP-ZF@CN nanocomposite

A simple polycondensation method was used to synthesize CN. Briefly, urea and dicyandiamide were prepared in a 40:20 g (2:1) mass ratio and ground in a mortar. The resulting powder was transferred to a container and heated in a muffle furnace to 550°C for four hours at a heating rate of 2°C per minute. Afterward, the sample was permitted to cool spontaneously to room temperature. The resulting yellow solid was then ground into a yellow powder. Subsequently, the CN powder underwent thermal exfoliation through the calcination method at 520°C for two hours. Finally, the exfoliated CN (2DCN) was successfully synthesized, appearing as a pale-yellow solid. The product was collected, ground into a fine powder, and stored for further use.

The OP-ZF@CN nanocomposite was synthesized by initially creating a mixture of 4.848 g of iron nitrate and 1.782 g of zinc nitrate in a 30 mL solution of ethanol and isopropyl alcohol, combined in a 1:1 (v/v) ratio. Then, 2.4 g (60 mmol) of 5 M NaOH was added to the precipitate ZF. Subsequently, 300 mg of 2DCN was added to the solution and stirred until uniformly dispersed. The prepared sample was transferred into a Teflon-lined autoclave with a maximum capacity of 50 mL and heated to 160°C for 16 hours. The resulting OP-ZF@CN nanocomposite was rinsed with distilled water and then filtered. The OP-ZF@CN nanocomposites were dried overnight at 60°C.

2.3 Characterization of OP-ZF@CN nanocomposite

The morphology and microstructure were examined using a JEOL JSM-6490LV SEM. The crystal structure was analyzed using Bruker D8 Advance XRD with a wavelength of 1.5406 Å over a 2θ range of 10°–80°. UV-Vis spectrophotometry Hitachi U-4100 was used to obtain the absorption spectrum within the 350–800 nm range. Fourier-transform infrared spectroscopy Nicolet 6700 was utilized to analyze the functional groups of the photocatalytic material using the KBr method.

2.4 Photocatalytic degradation experiments

A handmade photoreactor was used to evaluate the photocatalytic degradation of enrofloxacin. Briefly, 2.5 mg of photocatalyst was accurately weighed and added to 10 mL of enrofloxacin

solution (10 mg L⁻¹). Prior to irradiation, the enrofloxacin solution and photocatalyst mixture were stirred in the dark for 10 minutes to reach adsorption equilibrium. The solution was irradiated with eight visible light lamps (64 W) at a wavelength of 460 nm, and 1 mL samples were collected at five-minute intervals. The collected samples were centrifuged for five minutes and then filtered using a 0.22 μm PTFE membrane. The remaining residue was analyzed using HPLC with a C-18 column. The pH levels were regulated by the addition of 0.1 M hydrochloric acid and/or sodium hydroxide to the solution.

2.5 Model of Adsorption Kinetics and Isotherm

The adsorption kinetics are affected by several factors, such as the order of the reaction, the capacity for adsorption, and the rate at which adsorption occurs. The kinetic models for pseudo-first-order (PFO) and pseudo-second-order (PSO) reactions were employed to evaluate the adsorption of ENR on the surface of OP-ZF@CN and characterize the dynamics of adsorption by using the linear forms of these models—PFO (Equation 1) and PSO (Equation 2).

$$\ln(q_e - q_t) = \ln q_e - K_1 t \quad (1)$$

$$\frac{t}{q_t} = \frac{1}{K_2 + q_e^2} + \frac{1}{q_e} t \quad (2)$$

In these equations, q_t denotes the quantity of ENR adsorbed at a specific time, while q_e represents the equilibrium adsorption capacity (mg g⁻¹). The rate constants for PFO (min⁻¹) and PSO (mg g⁻¹ min⁻¹) are represented by the constants K_1 and K_2 , respectively. Furthermore, the isotherm of the adsorption model shed light on the distribution of ENR molecules at the liquid-solid interface during equilibrium, indicating whether this distribution was homogeneous or heterogeneous. This model also revealed information about the active sites and whether the adsorption occurred in a monolayer or multilayer format. To further explore the adsorption mechanism of the photocatalytic adsorbent, the nonlinear Sips model (Eq. 3) was applied.

$$q_e = \frac{K_a(C_e)^n}{1 + K_a(C_e)^n} q_m \quad (3)$$

In these equations, the adsorption capacity (L mg⁻¹) and intensity are represented by the

constants K_a and n , respectively. Together, these models offer a thorough understanding of how the nanocomposite adsorbents interact with ENR throughout the adsorption process.

3. Result and Discussion

The XRD patterns of the OP-ZF@CN nanocomposite are illustrated in Figure 1a. The distinctive diffraction peaks for pure 2DCN and ZF were identified at 2θ values of 27.5° and 35.5° , which corresponded to the highest peak in 2DCN and ZF, respectively [22,23]. These peaks corresponded to the Joint Committee on Powder Diffraction Standards (JCPDS) cards No. 87-1526 for 2DCN and No. 89-1010 for ZF, confirming the high crystallinity and purity of the samples. The absence of any impurity phases further highlighted the crystalline nature of both 2DCN and ZF. For the OP-ZF@CN nanocomposite, additional diffraction peaks were detected at 127° , 27.4° , 29.6° , 35.6° , 42.4° , 53.2° , 56.6° , and 62.5° , which corresponded to the crystallographic planes (100), (002), (220), (311), (400), (422), (511), and (440), respectively

[24-26]. Notably, the reduced intensity of the (002) peak in 2DCN was attributed to the incorporation of ZF nanoparticles onto the surface of 2DCN.

Figure 1b presents the FT-IR spectra for 2DCN, ZF, and the OP-ZF@CN nanocomposite. In the case of 2DCN, the stretching vibrational modes of the C-N heterocycles (heptazine units) appeared in the range of $1,150$ – $1,700$ cm^{-1} , with a distinct peak at 812 cm^{-1} that was attributed to the heptazine rings of 2DCN. N-H stretching vibrations were observed between $3,000$ and $3,500$ cm^{-1} . For ZF, both the inverse and normal spinel structures showed two distinct active modes of infrared at 562.2 and 433.5 cm^{-1} . These modes were associated with Fe-O and Zn-O bonds, corresponding to the octahedral and tetrahedral sites, respectively [27,28]. Additionally, absorption bands at $1,636$ cm^{-1} were attributed to the bending of surface hydroxyl groups on ZF [29]. The OP-ZF@CN nanocomposite showed absorption peaks at 813 , $1,245$, $1,416$, and $1,557$ cm^{-1} , indicating stronger absorption and suggesting changes in the coordination environment of 2DCN due to its interaction with ZF.

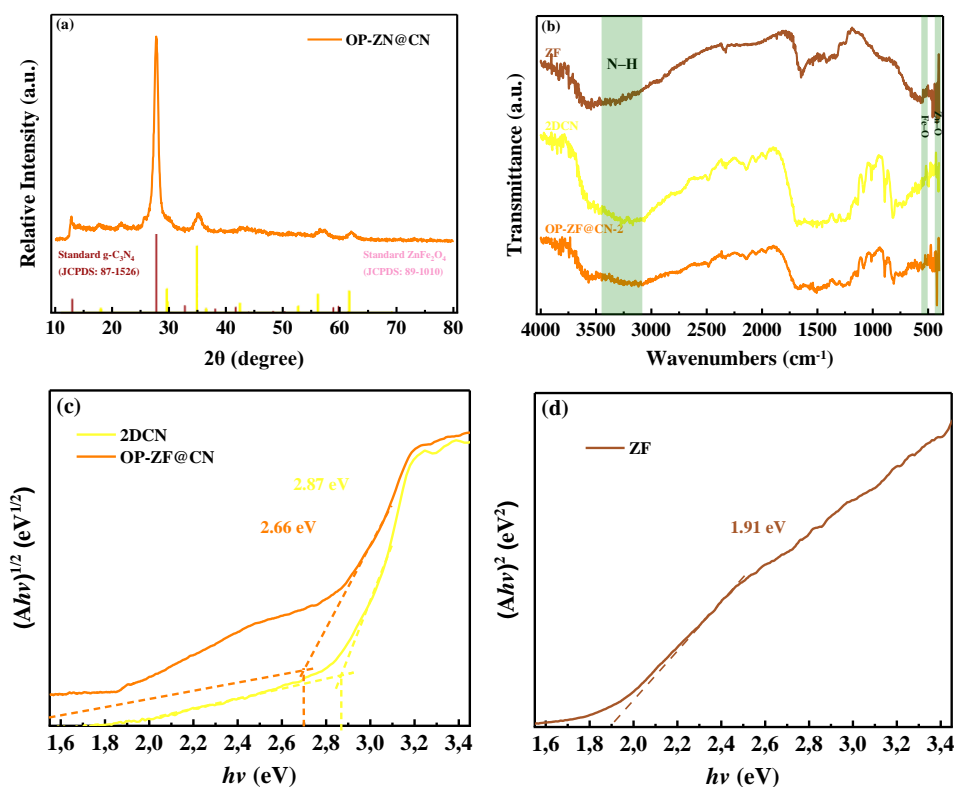


Fig. 1. (a) X-Ray diffraction pattern, (b) FT-IR spectra, and (c-d) Tauc plot of 2DCN, ZF, and OP-ZF@CN nanocomposite.

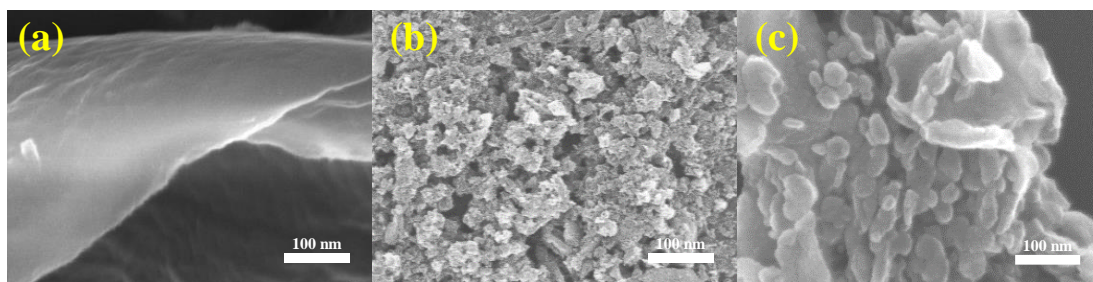


Fig. 2. SEM images of (a) 2DCN, (b) ZF, and (c) OP-ZF@CN nanocomposite.

The optical bandgap of the samples was examined by diffuse reflectance spectroscopy (DRS). Utilizing the Tauc function, the calculated bandgaps were 2.8 eV for 2DCN, 1.9 eV for ZF, and 2.6 eV for the OP-ZF@CN nanocomposite. Figures 1c and 1d show that both 2DCN and OP-ZF@CN had indirect band gaps, while pure ZF demonstrated a direct semiconductor band gap [30,31]. The OP-ZF@CN nanocomposite exhibited a wider absorption spectrum in the visible light range compared to pristine 2DCN, which could potentially improve the generation of electron-hole pairs (e^-h^+).

Morphological and elemental composition analyses, including assessments of particle shape and size distribution, were performed using SEM. Figure 2a presents SEM images of 2DCN, revealing its sheet-like structure, while Figure 2b shows ZF nanoparticles with a spherical shape and an average size of 20 nm. Figure 2c shows the even distribution of ZF particles on the surface of 2DCN. These results validated the formation of the OP-ZF@CN heterojunction.

Enrofloxacin Degradation through Synergistic Adsorption-Photocatalysis

The synergistic effects of adsorption and photocatalytic degradation of enrofloxacin using the OP-ZF@CN nanocomposite were assessed under both dark and light conditions. The adsorption tests were conducted in the dark with a 10 mg L^{-1} ENR solution (10 mL, pH 7, and 0.25 g L^{-1} adsorbate) to eliminate any influence from photocatalysis. Equilibrium and saturation were achieved within 30 minutes, with rapid adsorption occurring in the first 10 minutes, followed by a slower rate until saturation. The OP-ZF@CN nanocomposite demonstrated a maximum adsorption capacity of 11.08 mg g^{-1} , while pure

2DCN had a capacity of 8.26 mg g^{-1} , corresponding to 28% and 21% removal of ENR, respectively. In contrast, ZF removed only 16% of ENR, with a maximum adsorption capacity of 6.56 mg g^{-1} . Figure 3a illustrates the ENR adsorption capacity (q_t) of the OP-ZF@CN nanocomposite.

The adsorption capacity surged to 8.61 mg g^{-1} within the first 10 minutes, indicating rapid uptake of ENR by OP-ZF@CN. Afterward, the rate of adsorption slowed, and equilibrium was reached after 30 minutes, as no additional ENR could be adsorbed. The pseudo-first-order and pseudo-second-order models were used to simulate the adsorption process, with their fitting curves shown in Figure 3a. The results indicated that the adsorption rate was initially high but gradually slowed after 10 minutes, with ENR uptake reaching saturation after 30 minutes, suggesting that the adsorption process was completed quickly. This swift process might be attributed to the mesoporous structure of OP-ZF@CN, which minimized the diffusion resistance for the ENR molecules. Table 1 presents various parameters for the isotherm and kinetic model results of the OP-ZF@CN nanocomposite. According to the results in Table 1, the pseudo-first-order model ($R^2 = 0.9891$) demonstrated a better fit compared to the pseudo-second-order model ($R^2 = 0.9214$), suggesting that the pseudo-first-order model more accurately represents the adsorption process. The pseudo-first-order model assumes that the adsorption rate is influenced by the square of the number of vacant sites occupied by adsorbates and is primarily governed by physical interactions. The good fit of the pseudo-first-order model to the experimental data suggested that the process was likely physisorption, involving weak van der Waals forces [32].

Table 1. Isotherm and kinetic model result of the OP-ZF@CN nanocomposite.

Model	Parameter	Value	R ²
Isotherm			
Langmuir	q _m (mg g ⁻¹)	73.63	0.9946
	K _L (L mg ⁻¹)	0.028	
Freundlich	K _F ((mg g ⁻¹)/(L mg ⁻¹) ^{1/n})	3.43	0.9826
	1/n	1.51	
Sips	q _m (mg g ⁻¹)	62.23	0.9953
	K _S (L mg ⁻¹)	0.038	
	γ	1.12	
Kinetic			
Pseudo-1st-order	K ₁ (min ⁻¹)	0.158	0.9891
	q _e (mg g ⁻¹)	11.08	
Pseudo-2nd-order	K ₂ (g (mg·min) ⁻¹)	0.018	0.9214
	q _e (mg g ⁻¹)	12.41	

The narrow bandgap energy of ZF (1.91 eV) caused substantial recombination of electron-hole (e⁻-h⁺) pairs, resulting in the lowest photocatalytic performance among all the materials tested, achieving only 33% degradation within 30 minutes under visible light exposure (Figure 3b). Conversely, 2DCN and OP-ZF@CN showed superior photodegradation, with 50% and 99% removal of ENR, respectively. The enhanced performance of OP-ZF@CN can be attributed to its lower bandgap energy (2.66 eV) compared to that of pure 2DCN (2.87 eV), enabling more efficient utilization of visible light while reducing the recombination rate of electron-hole (e⁻-h⁺) pairs. The photodegradation of ENR followed pseudo-first-order kinetics, with OP-ZF@CN exhibiting optimal performance due to the synergistic interaction between adsorption and photocatalysis. In the OP-ZF@CN nanocomposite, ENR molecules were readily adsorbed and concentrated on the lamellar structure of carbon nitride nanosheets (2DCN), which offered a high surface area and numerous mesoporous sites. This setup promoted a rapid reduction in ENR concentration in the solution, increasing the likelihood of interactions between ENR and the nanocomposite, thereby enhancing photodegradation through the generation of reactive oxygen species. These findings confirmed that the heterojunction formed between ZF and 2DCN significantly boosted photocatalytic activity, making the OP-ZF@CN nanocomposite a highly

effective material for ENR degradation. Kinetic studies were conducted to analyze the rate of degradation to understand the performance of the OP-ZF@CN nanocomposite better. The photodegradation of ENR followed pseudo-first-order kinetics, which is a common model for photocatalytic degradation processes. The reaction rate constant (*k*) for OP-ZF@CN was found to be 0.1321 min⁻¹, which was approximately 10 times higher than that of 2DCN (0.0127 min⁻¹) and ZF (0.0072 min⁻¹). This significant increase in the reaction rate constant demonstrated the exceptional photocatalytic efficiency of OP-ZF@CN and underscored the importance of the synergistic interaction between the two components of the composite.

pH is an important environmental parameter in the processes of adsorption and photodegradation of various pollutants. Therefore, this study also investigates the effect of pH on the ENR solution, which not only affects the surface charge of the OP-ZF@CN nanocomposite but also influences the speciation of ENR in the solution. ENR has two dissociation constants, pKa₁ = 6.1 and pKa₂ = 7.7, which indicate different ionic forms depending on the pH of the solution [33]. The species of ENR formed are cationic (ENR⁺) at pH < 6.1, zwitterionic (ENR^z) in the pH range of 6.1 to 7.7, and anionic (EFA⁻) at pH > 7.7. These species structures are associated with piperazine, carboxyl, and amine groups. Increased adsorption and

photodegradation efficiency can be seen in Figure 4a, where the removal efficiency was 67% at pH 5 and 99% at pH 7. However, photodegradation of ENR decreased when the pH rose to 9 (75%). This

indicated that both highly acidic and alkaline conditions reduced the photodegradation capability of the OP-ZF@CN nanocomposite towards ENR [34].

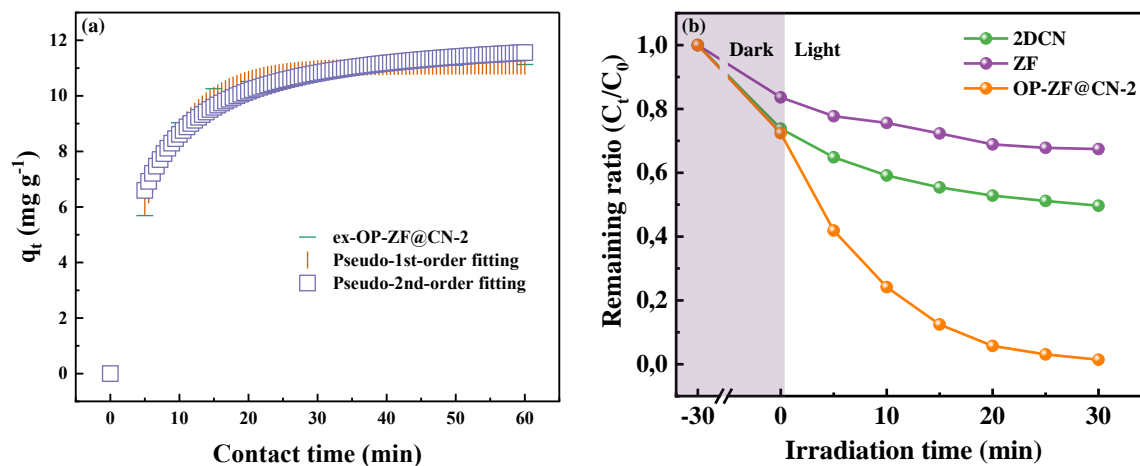


Fig. 3. (a) The adsorption kinetic of OP-ZF@CN nanocomposite and (b) the photocatalytic performance of 2DCN, ZF, and the OP-ZF@CN nanocomposite.

Furthermore, the zeta potential results shown in Figure 4b indicate that the OP-ZF@CN nanocomposite exhibited a negative charge in the pH range of 4.4 to 11. Based on this zeta potential data, the removal of ENR by the OP-ZF@CN nanocomposite corresponded to the effect of the zeta potential, where a neutral environment was conducive to the effective treatment of ENR by the OP-ZF@CN nanocomposite with optimal electrostatic forces during the photodegradation process [35]. Additionally, the free amine group ($-NH_2$) in the OP-ZF@CN nanocomposite and the electronegative atoms of ENR (N, O, and F) induced the formation of hydrogen bonds, supporting the removal of ENR. Moreover, the increased photocatalytic degradation at pH 7 could be attributed to the more negative surface charge of OP-ZF@CN. On the other hand, the reduced ENR removal at pH 9 was associated with the negative charge of ENR, which caused repulsive interactions with the OP-ZF@CN nanocomposite. Furthermore, the adsorption capacity of the OP-ZF@CN nanocomposite was evaluated by studying the interaction between the composite and ENR at different concentrations. The adsorption tests were conducted using a range of initial ENR concentrations, from 5 to 50 mg L⁻¹. The results showed that the adsorption capacity of OP-ZF@CN increased with higher ENR concentrations until a

saturation point was reached. A contact time of 30 minutes was sufficient to reach adsorption equilibrium, with the equilibrium capacities of the nanocomposite being 6.53, 11.33, 21.09, 28.64, 35.57, and 37.79 mg g⁻¹ for ENR concentrations of 5, 10, 20, 30, 40, and 50 mg L⁻¹, respectively. This increase in adsorption capacity with higher concentrations of ENR demonstrated the effectiveness of OP-ZF@CN in capturing and concentrating the pollutant molecules, which enhanced the subsequent photocatalytic degradation process. The calculated reaction rate constants for 2DCN, ZF, and OP-ZF@CN were 0.0127, 0.0072, and 0.1321 min⁻¹, respectively, indicating that the OP-ZF@CN nanocomposite excelled in ENR removal, achieving a rate 10 times higher than that of pure 2DCN.

Adsorption isotherms are essential for understanding the interactions between OP-ZF@CN and ENR, which are critical for optimizing adsorbent efficiency. The isotherm study was conducted using a material prepared at a concentration of 0.25 g L⁻¹, which was added to a 10 mL enrofloxacin solution with a concentration range of 5-50 mg L⁻¹ at neutral pH. The experiment was carried out with a contact time of 30 minutes. In this study, there are three isotherm models, namely Langmuir, Freundlich, and Sips, were employed to explore the interactions between OP-

ZF@CN and ENR. The non-linear fits for these models are displayed in Figure 4c, with their parameters and R^2 values shown in Table 1. The R^2 values were ranked as Sips (0.9953) > Langmuir (0.9946) > Freundlich (0.9826), indicating that the Sips and Langmuir models better described ENR adsorption on OP-ZF@CN. The isotherm curve showed a steady increase with higher C_e , and the Sips model predicted a q_m of 62.23 mg g^{-1} , indicating that greater initial concentrations of ENR could be effectively absorbed by the OP-ZF@CN nanocomposite. Additionally, the

adsorption process was not confined to a single layer of sorption, as interactions between the adsorbed ENR molecules might take place, evidenced by a γ value of 1.1. Moreover, The Sips model was utilized to analyze the characteristics of the adsorption process and to establish the optimum adsorption capacity. This model represented a combination of the Langmuir and Freundlich models for heterogeneous systems, demonstrating an R^2 value of 0.9953 and a maximum adsorption capacity of 62.23 mg g^{-1} .

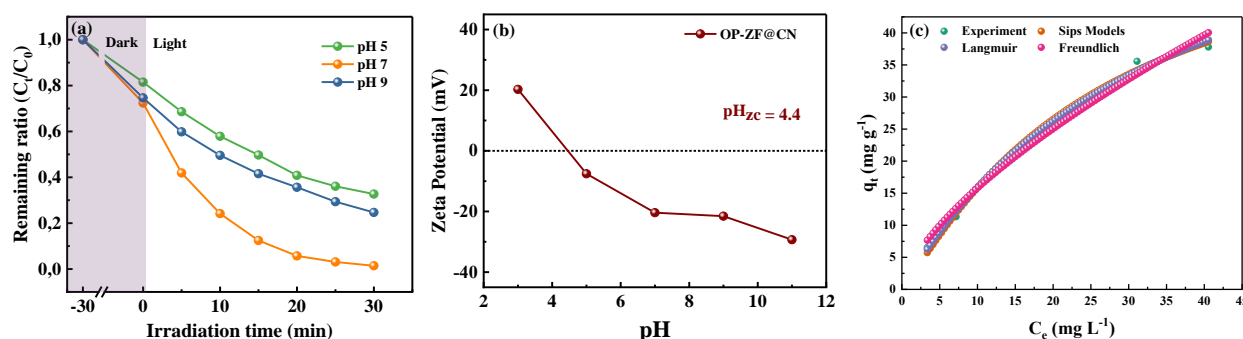


Fig. 4. (a) The effect of pH toward ENR removal efficiency by OP-ZF@CN, (b) zeta potential value of OP-ZF@CN, and (c) the Sips isotherm exponential fitting.

These results confirmed that the adsorption of ENR on OP-ZF@CN included heterogeneous active sites and followed a multilayer adsorption process. According to Gile and Smith's classification of solute adsorption isotherms, the OP-ZF@CN nanocomposite conformed to an L2 type isotherm, implying a strong affinity between ENR and the OP-ZF@CN nanocomposite, facilitated by chemical bonding or electrostatic interactions that occurred during the multilayer adsorption process [36,37].

4. Conclusions

The results of this study provide compelling evidence that the OP-ZF@CN nanocomposite is an effective material for the dual removal of enrofloxacin (ENR) from aqueous solutions, combining both adsorption and photocatalytic degradation processes. The adsorption capacity of OP-ZF@CN was significantly higher than that of pure 2DCN and ZF, with a maximum adsorption capacity of 62.23 mg g^{-1} , as determined by the Sips isotherm model. This value was indicative of the nanocomposite's high affinity for ENR, which was facilitated by the heterogeneous active sites within the material's structure. The adsorption process

was rapid, reaching equilibrium within 30 minutes, and it followed pseudo-first-order kinetics, suggesting that the adsorption mechanism was dominated by physical interactions, likely due to weak van der Waals forces. Furthermore, the Sips isotherm model revealed a multilayer adsorption process, confirming the complex interaction between the ENR molecules and the nanocomposite. The photocatalytic degradation of ENR under visible light exposure also showed exceptional performance. The OP-ZF@CN nanocomposite achieved a 99% degradation of ENR in 30 minutes, outperforming both pure 2DCN (50% degradation) and ZF (33% degradation). The improvement in photocatalytic performance could be attributed to the formation of a heterojunction between zinc ferrite (ZF) and $g\text{-C}_3\text{N}_4$ (2DCN), which reduced the electron-hole recombination rate and enhanced light absorption. This synergy enabled OP-ZF@CN to utilize visible light more effectively, leading to a 10-fold increase in the photocatalytic reaction rate compared to pure 2DCN. The reaction rate constant for OP-ZF@CN was 0.1321 min^{-1} , a significant improvement over the values observed for pure ZF (0.0072 min^{-1}) and

2DCN (0.0127 min^{-1}). The characterization of the OP-ZF@CN nanocomposite using techniques such as XRD, FT-IR, and SEM confirmed the successful synthesis of the heterostructure. The XRD patterns indicated high crystallinity, and the FT-IR spectra revealed characteristic functional groups associated with both 2DCN and ZF. The SEM images showed an even distribution of ZF nanoparticles on the surface of 2DCN, validating the formation of the heterojunction and confirming the morphology conducive to both adsorption and photocatalytic processes.

Acknowledgments

The author would like to express gratitude to Direktorat Riset dan Pengabdian Masyarakat, Deputi Bidang Penguatan Riset dan Pengembangan, Kementerian Pendidikan, Kebudayaan, and Riset dan Teknologi for their financial support in accordance with the 2024 Fiscal Year Research Contract Number: 109/E5/PG.02.00.PL/2024.

References

- [1] Zhou, P., Wang, Y., Yan, X., Gan, Y., Xia, C., Xu, Y., Xie, M. (2024). Nitrogen-defect-modified $g\text{-C}_3\text{N}_4/\text{BaFe}_{12}\text{O}_{19}$ S-scheme heterojunction photocatalyst with enhanced advanced oxidation technology synergistic photothermal degradation ability of antibiotic: Insights into performance, electron transfer pathways and toxicity. *Applied Catalysis B: Environmental*, 343 123485. <https://doi.org/10.1016/j.apcatb.2023.123485>
- [2] Sha, J., Li, L., An, Z., He, M., Yu, H., Wang, Y., Gao, B., Xu, S. (2022). Diametrically opposite effect of Cu^{2+} on sulfamerazine and ciprofloxacin adsorption-photodegradation in $g\text{-C}_3\text{N}_4/\text{visible light}$ system: behavior and mechanism study. *Chemical Engineering Journal*, 428 131065. <https://doi.org/10.1016/j.cej.2021.131065>
- [3] Rafieenia, R., Sulonen, M., Mahmoud, M., El-Gohary, F., Rossa, C. A. (2022). Integration of microbial electrochemical systems and photocatalysis for sustainable treatment of organic recalcitrant wastewaters: Main mechanisms, recent advances, and present prospects. *Science of The Total Environment*, 824 153923. <https://doi.org/10.1016/j.scitotenv.2022.153923>
- [4] Hu, X., Yu, Y., Chen, D., Xu, W., Fang, J., Liu, Z., Li, R., Yao, L., Qin, J., Fang, Z. (2022). Anatase/Rutile homojunction quantum dots anchored on $g\text{-C}_3\text{N}_4$ nanosheets for antibiotics degradation in seawater matrix via coupled adsorption-photocatalysis: Mechanism insight and toxicity evaluation. *Chemical Engineering Journal*, 432 134375. <https://doi.org/10.1016/j.cej.2021.134375>
- [5] Wang, P., Tang, Y., Dong, Z., Chen, Z., Lim, T.-T. (2013). Ag-AgBr/TiO₂/RGO nanocomposite for visible-light photocatalytic degradation of penicillin G. *Journal of Materials Chemistry A*, 1(15), 4718-4727. <https://doi.org/10.1039/C3TA01042B>
- [6] Zhang, R., Jiang, J., Zeng, K. (2022). Synthesis of $\text{Bi}_2\text{WO}_6/g\text{-C}_3\text{N}_4$ heterojunction on activated carbon fiber membrane as a thin-film photocatalyst for treating antibiotic wastewater. *Inorganic Chemistry Communications*, 140 109418. <https://doi.org/10.1016/j.inoche.2022.109418>
- [7] Zhang, J., Zheng, Y., Zheng, H., Jing, T., Zhao, Y., Tian, J. (2022). Porous Oxygen-Doped $g\text{-C}_3\text{N}_4$ with the Different Precursors for Excellent Photocatalytic Activities under Visible Light. *Materials*, 15(4). <https://doi.org/10.3390/ma15041391>
- [8] Isloor, A. M., O, S., martis, G. J., Bhat, S. P., Mugali, P. (2024). Impact of TiO₂ and CaCO₃ nanoparticles and their incorporation in polysulfone composite membrane on photocatalytic degradation of RB 5. *Advances in Environmental Technology*, 10(4), 315-325. <https://doi.org/10.22104/aet.2024.6957.1907>
- [9] Dang, V. D., Adorna, J., Annadurai, T., Bui, T. A. N., Tran, H. L., Lin, L.-Y., Doong, R.-A. (2021). Indirect Z-scheme nitrogen-doped carbon dot decorated $\text{Bi}_2\text{MoO}_6/g\text{-C}_3\text{N}_4$ photocatalyst for enhanced visible-light-driven degradation of ciprofloxacin. *Chemical Engineering Journal*, 422 130103. <https://doi.org/10.1016/j.cej.2021.130103>
- [10] Chen, P., Di, S., Qiu, X., Zhu, S. (2022). One-step synthesis of F-TiO₂/ $g\text{-C}_3\text{N}_4$ heterojunction

- as highly efficient visible-light-active catalysts for tetrabromobisphenol A and sulfamethazine degradation. *Applied Surface Science*, 587 152889.
<https://doi.org/10.1016/j.apsusc.2022.152889>
- [11] Abdul kader, H. D., Ammar, S. H., Abdalnabi, W. A., Jabbar, Z. H., Taofeeq, H., Al-Farraj, A. (2024). Enhancing visible-light-based photodegradation of antibiotics over facile constructed BiVO₄/S-doped g-C₃N₄ heterojunctions in an airlift photocatalytic reactor. *Journal of Water Process Engineering*, 65 105900.
<https://doi.org/10.1016/j.jwpe.2024.105900>
- [12] Liu, R., Zhang, C., Liu, R., Sun, Y., Ren, B., Tong, Y., Tao, Y. (2025). Advancing antibiotic detection and degradation: recent innovations in graphitic carbon nitride (g-C₃N₄) applications. *Journal of Environmental Sciences*, 150 657-675.
<https://doi.org/10.1016/j.jes.2024.03.033>
- [13] Alaghmandfard, A., Ghandi, K. (2022). A comprehensive review of graphitic carbon nitride (g-C₃N₄)-metal oxide-based nanocomposites: potential for photocatalysis and sensing. *Nanomaterials*, 12(2).
<https://doi.org/10.3390/nano12020294>
- [14] Mafa, P. J., Malefane, M. E., Idris, A. O., Liu, D., Gui, J., Mamba, B. B., Kuvarega, A. T. (2022). Multi-elemental doped g-C₃N₄ with enhanced visible light photocatalytic Activity: Insight into naproxen Degradation, Kinetics, effect of Electrolytes, and mechanism. *Separation and Purification Technology*, 282 120089.
<https://doi.org/10.1016/j.seppur.2021.120089>
- [15] Deng, X., Wang, D., Li, H., Jiang, W., Zhou, T., Wen, Y., Yu, B., Che, G., Wang, L. (2022). Boosting interfacial charge separation and photocatalytic activity of 2D/2D g-C₃N₄/ZnIn₂S₄ S-scheme heterojunction under visible light irradiation. *Journal of Alloys and Compounds*, 894 162209.
<https://doi.org/10.1016/j.jallcom.2021.162209>
- [16] Lu, N., Wang, P., Su, Y., Yu, H., Liu, N., Quan, X. (2019). Construction of Z-Scheme g-C₃N₄/RGO/WO₃ with in situ photoreduced graphene oxide as electron mediator for efficient photocatalytic degradation of ciprofloxacin. *Chemosphere*, 215 444-453.
<https://doi.org/10.1016/j.chemosphere.2018.10.065>
- [17] Tian, C., Zhao, H., Sun, H., Xiao, K., Keung Wong, P. (2020). Enhanced adsorption and photocatalytic activities of ultrathin graphitic carbon nitride nanosheets: Kinetics and mechanism. *Chemical Engineering Journal*, 381 122760.
<https://doi.org/10.1016/j.cej.2019.122760>
- [18] Zhang, Y., Chen, S., Meng, Y., Chang, L., Huang, X., Zheng, Y., Shen, J., Zhao, T. (2022). CNTs boosting superior cycling stability of ZnFe₂O₄/C nanoparticles as high-capacity anode materials of Li-ion batteries. *Journal of Alloys and Compounds*, 912 165135.
<https://doi.org/10.1016/j.jallcom.2022.165135>
- [19] Yang, H., Hao, H., Zhao, Y., Hu, Y., Min, J., Zhang, G., Bi, J., Yan, S., Hou, H. (2022). An efficient construction method of S-scheme Ag₂CrO₄/ZnFe₂O₄ nanofibers heterojunction toward enhanced photocatalytic and antibacterial activity. *Colloids and Surfaces A: Physicochemical and Engineering Aspects*, 641 128603.
<https://doi.org/10.1016/j.colsurfa.2022.128603>
- [20] Wu, X., Lu, J., Huang, S., Shen, X., Cui, S., Chen, X. (2022). Facile fabrication of novel magnetic 3-D ZnFe₂O₄/ZnO aerogel based heterojunction for photoreduction of Cr(VI) under visible light: Controlled synthesis, facial change distribution, and DFT study. *Applied Surface Science*, 594 153486.
<https://doi.org/10.1016/j.apsusc.2022.153486>
- [21] Luo, J., Wu, Y., Chen, X., He, T., Zeng, Y., Wang, G., Wang, Y., Zhao, Y., Chen, Z. (2022). Synergistic adsorption-photocatalytic activity using Z-scheme based magnetic ZnFe₂O₄/CuWO₄ heterojunction for tetracycline removal. *Journal of Alloys and Compounds*, 910 164954.
<https://doi.org/10.1016/j.jallcom.2022.164954>
- [22] Wang, S., Wang, J. (2022). Magnetic 2D/2D oxygen doped g-C₃N₄/biochar composite to activate peroxymonosulfate for degradation of emerging organic pollutants. *Journal of Hazardous Materials*, 423 127207.
<https://doi.org/10.1016/j.jhazmat.2021.127207>

- [23] Wu, Y., Chen, J., Che, H., Gao, X., Ao, Y., Wang, P. (2022). Boosting $2e^-$ oxygen reduction reaction in garland carbon nitride with carbon defects for high-efficient photocatalysis-self-Fenton degradation of 2,4-dichlorophenol. *Applied Catalysis B: Environment and Energy*, 307 121185. <https://doi.org/10.1016/j.apcatb.2022.121185>
- [24] Nguyen, T. B., Huang, C. P., Doong, R.-a. (2019). Photocatalytic degradation of bisphenol A over a $ZnFe_2O_4/TiO_2$ nanocomposite under visible light. *Science of The Total Environment*, 646 745-756. <https://doi.org/10.1016/j.scitotenv.2018.07.352>
- [25] Al-Sulami, A. I., Alsuwat, M. H., AlSulami, F. M. H., Ibrahim, A. M., Elhenawy, A. A. (2024). $ZnFe_2O_4$ /bentonite/polyacrylamide: Exploring structural properties for removal of Alizarin Yellow Dye and antibacterial activities. *Colloids and Surfaces A: Physicochemical and Engineering Aspects*, 687 133408. <https://doi.org/10.1016/j.colsurfa.2024.133408>
- [26] Al-Shwaiman, H. A., Akshhaya, C., Syed, A., Bahkali, A. H., Elgorban, A. M., Das, A., Varma, R. S., Khan, S. S. (2022). Fabrication of intimately coupled $CeO_2/ZnFe_2O_4$ nano-heterojunction for visible-light photocatalysis and bactericidal application. *Materials Chemistry and Physics*, 279 125759. <https://doi.org/10.1016/j.matchemphys.2022.125759>
- [27] Matli, P. R., Zhou, X., Shiyu, D., Huang, Q. (2015). Fabrication, characterization, and magnetic behavior of porous $ZnFe_2O_4$ hollow microspheres. *International Nano Letters*, 5(1), 53-59. <https://doi.org/10.1007/s40089-014-0135-2>
- [28] Nguyen, T. B., Doong, R.-a. (2017). Heterostructured $ZnFe_2O_4/TiO_2$ nanocomposites with a highly recyclable visible-light-response for bisphenol A degradation. *RSC Advances*, 7(79), 50006-50016. <https://doi.org/10.1039/C7RA08271A>
- [29] Sarala, E., Madhukara Naik, M., Vinuth, M., Rami Reddy, Y. V., Sujatha, H. R. (2020). Green synthesis of Lawsonia inermis-mediated zinc ferrite nanoparticles for magnetic studies and anticancer activity against breast cancer (MCF-7) cell lines. *Journal of Materials Science: Materials in Electronics*, 31(11), 8589-8596. <https://doi.org/10.1007/s10854-020-03394-8>
- [30] Sarkar, P., De, S., Neogi, S. (2022). Microwave assisted facile fabrication of dual Z-scheme $g-C_3N_4/ZnFe_2O_4/Bi_2S_3$ photocatalyst for peroxymonosulphate mediated degradation of 2,4,6-Trichlorophenol: The mechanistic insights. *Applied Catalysis B: Environment and Energy*, 307 121165. <https://doi.org/10.1016/j.apcatb.2022.121165>
- [31] Shi, Y., Li, L., Xu, Z., Sun, H., Amin, S., Guo, F., Shi, W., Li, Y. (2022). Engineering of 2D/3D architectures type II heterojunction with high-crystalline $g-C_3N_4$ nanosheets on yolk-shell $ZnFe_2O_4$ for enhanced photocatalytic tetracycline degradation. *Materials Research Bulletin*, 150 111789. <https://doi.org/10.1016/j.materresbull.2022.111789>
- [32] Zhou, Q., Chen, W., Jiang, X., Liu, H., Ma, S., Wang, B. (2020). Preparation of a novel nitrogen-containing graphitic mesoporous carbon for the removal of acid red 88. *Scientific reports*, 10(1), 1353. <https://doi.org/10.1038/s41598-020-57823-z>
- [33] Xiao, Y., Lyu, H., Tang, J., Wang, K., Sun, H. (2020). Effects of ball milling on the photochemistry of biochar: Enrofloxacin degradation and possible mechanisms. *Chemical Engineering Journal*, 384 123311. <https://doi.org/10.1016/j.cej.2019.123311>
- [34] Wang, W., Zhang, J., Chen, T., Sun, J., Ma, X., Wang, Y., Wang, J., Xie, Z. (2020). Preparation of TiO_2 -modified biochar and its characteristics of photo-catalysis degradation for enrofloxacin. *Scientific reports*, 10(1), 6588. <https://doi.org/10.1038/s41598-020-62791-5>
- [35] Cai, M., Liu, Y., Wang, C., Lin, W., Li, S. (2023). Novel $Cd_{0.5}Zn_{0.5}S/Bi_2MoO_6$ S-scheme heterojunction for boosting the photodegradation of antibiotic enrofloxacin: Degradation pathway, mechanism and toxicity assessment. *Separation and Purification Technology*, 304 122401. <https://doi.org/10.1016/j.seppur.2022.122401>
- [36] Abbasi, M. A., Amin, K. M., Ali, M., Ali, Z., Atif, M., Ensinger, W., Khalid, W. (2022). Synergetic effect of adsorption-photocatalysis by $GO-CeO_2$ nanocomposites for photodegradation of doxorubicin. *Journal of*

Environmental Chemical Engineering, 10(1), 107078.

<https://doi.org/10.1016/j.jece.2021.107078>

- [37] Wang, P., Wang, X., Yu, S., Zou, Y., Wang, J., Chen, Z., Alharbi, N. S., Alsaedi, A., Hayat, T., Chen, Y., Wang, X. (2016). Silica coated Fe₃O₄

magnetic nanospheres for high removal of organic pollutants from wastewater. Chemical Engineering Journal, 306 280-288.

<https://doi.org/10.1016/j.cej.2016.07.068>

How to cite this paper:



Tamyiz, M., Fitri, M. A., Azizah, Z., Asmarani, N. N. F. P. & Rahma, I. N. (2025). Easy One-Pot Synthesis of Zinc Ferrite@Graphitic Carbon Nitride for Combined Adsorption and Photocatalytic Degradation of Enrofloxacin Under Visible Light. Advances in Environmental Technology, 11(3) 2025, 254-265. DOI: 10.22104/aet.2025.7146.1966